buildings

MDPI

Article

A Multi-Objective Sensor Placement Method Considering Modal Identification Uncertainty and Damage Detection Sensitivity

Xue-Yang Pei [1], Yuan Hou [1], Hai-Bin Huang [2] and Jun-Xing Zheng [3,*]

[1] School of Civil Engineering, Yancheng Institute of Technology, Yancheng 224051, China
[2] School of Civil and Transportation Engineering, Hebei University of Technology, Tianjin 300401, China
[3] School of Civil and Hydraulic Engineering, Huazhong University of Science and Technology, Wuhan 430074, China
* Correspondence: junxing@hust.edu.cn

Abstract: Structural Health Monitoring relies on accurate modal identification and effective damage detection to assess structural performance and safety. However, traditional sensor placement methods struggle to balance modal identification uncertainty, which arises from limited sensor coverage and measurement noise and damage detection sensitivity, which requires sensors to be optimally positioned to capture structural stiffness variations. To address this challenge, this study proposes a multi-objective sensor placement optimization method based on the Non-Dominated Sorting Genetic Algorithm. The method introduces two key objective functions: minimizing modal identification uncertainty by leveraging Bayesian modal identification theory and information entropy and maximizing damage detection sensitivity by incorporating an entropy-based measure to quantify the uncertainty in stiffness variation estimation. By formulating the problem as Pareto-based multi-objective optimization, the method efficiently explores a trade-off between the two competing objectives and provides a diverse set of optimal sensor placement solutions. The proposed approach is validated through numerical experiments on a simply supported beam and a benchmark bridge structure, demonstrating that different optimization objectives lead to distinct sensor placement patterns. The results show that solutions prioritizing modal identification distribute sensors across the structure to improve global response estimation, while solutions favoring damage detection concentrate sensors in critical areas to enhance sensitivity. The proposed method significantly improves sensor placement strategies by offering a systematic and flexible framework for SHM applications, enabling engineers to tailor monitoring strategies based on specific structural assessment needs.

Keywords: multi-objective sensor placement; modal identification uncertainty; damage detection sensitivity; Pareto optimization; non-dominated sorting genetic algorithm

check for updates

Academic Editor: Humberto Varum

Received: 19 February 2025
Revised: 2 March 2025
Accepted: 3 March 2025
Published: 5 March 2025

Citation: Pei, X.-Y.; Hou, Y.; Huang, H.-B.; Zheng, J.-X. A Multi-Objective Sensor Placement Method Considering Modal Identification Uncertainty and Damage Detection Sensitivity. *Buildings* **2025**, *15*, 821. https://doi.org/10.3390/buildings15050821

Copyright: © 2025 by the authors. Licensee MDPI, Basel, Switzerland. This article is an open access article distributed under the terms and conditions of the Creative Commons Attribution (CC BY) license (https://creativecommons.org/licenses/by/4.0/).

1. Introduction

The safety and functionality of civil infrastructure are continuously assessed through Structural Health Monitoring (SHM) systems, which collect and analyze real-time structural response data to provide critical insights [1,2]. The accurate identification of modal parameters, such as natural frequencies, mode shapes, and modal coordinates, is a crucial component of SHM. These parameters play a key role in system identification, finite element model updating, and structural damage detection [3–5]. Structural damage is typically manifested as variations in these modal parameters, indicating potential changes in stiffness, mass, or damping characteristics [6]. However, the precision of modal parameter identification and damage detection is inherently constrained by the quality and

spatial distribution of sensor data, which can be affected by sensor placement limitations and measurement noise [7–9]. In practical engineering applications, such as bridges and high-rise buildings, researchers often need to develop optimized placement strategies for different types of sensors, including displacement and acceleration sensors, based on practical requirements and specific structural characteristics, in order to improve structural data collection [10–12]. Even when the number of sensors is limited, these strategies can still ensure accurate and consistent modal parameter identification.

The optimization of sensor placement for modal parameters has been widely explored in an effort to improve modal identification accuracy. This research primarily aims to minimize uncertainties stemming from modeling errors and measurement noise. Among these approaches, the Effective Independence (EI) method has emerged as a widely adopted strategy, selecting sensor locations by minimizing the Fisher information matrix's determinant, which is directly related to the covariance matrix of modal coordinate estimators [13]. This method has been further extended to support multidimensional sensor layouts, where multiple rows in the mode shape matrix are linked to a single sensor location [14]. Additionally, the relationship between the EI method and the kinetic energy (KE) method, which incorporates the mass matrix into the Fisher information matrix to enhance sensor selection criteria, has been explored [15]. Recent advancements have introduced Bayesian statistical frameworks into sensor placement optimization, leveraging probabilistic uncertainty modeling to improve robustness. In particular, information entropy has been proposed as a scalar metric for quantifying uncertainty, providing a rigorous theoretical basis for optimizing sensor configurations [16,17]. Furthermore, novel strategies integrating heterogeneous sensor types have been developed to enhance measurement accuracy. Pei et al. [18] proposed a hybrid placement method that optimizes the deployment of strain and acceleration sensors to minimize the uncertainty in displacement mode shape estimation. Similarly, Zhang and Xu [19] incorporated discrete Kalman filtering into sensor placement optimization, facilitating sensor arrangement strategies tailored for both response reconstruction and excitation reconstruction scenarios.

Damage detection-oriented sensor placement methods aim to strategically position sensors to enhance the identification of structural stiffness changes while improving modal identification accuracy. Among these approaches, frequency-based damage identification methods have been widely utilized due to their computational efficiency and simplicity. Early studies primarily relied on natural frequency shifts as indicators of structural damage [20,21]. However, compared to frequency-based approaches, mode shape analysis offers greater sensitivity to localized stiffness variations due to its spatially distributed characteristics [22,23].

To further refine damage detection, Yang [24] introduced information entropy as a measure to assess uncertainties arising from stiffness variations, treating them as model errors. Hiramoto et al. [25] applied the explicit solution of the algebraic Riccati equation to optimize both sensor and actuator placements for active vibration control, demonstrating an integrated approach to monitoring and control. Worden and Burrows [26] leveraged curvature data to develop novel sensor distribution methods, emphasizing the role of spatial derivatives in detecting structural anomalies. Additionally, Shi et al. [27] and Guo et al. [28] proposed sensor layouts specifically designed to detect and localize structural damage using test modal data, an area that remains relatively underexplored in sensor placement research. Further developments in damage-oriented sensor placement include the work of Pei et al. [29], who treated potential structural damage as modeling errors, adjusting sensor configurations to enhance modal identification. However, while their study optimized sensor placement for modal identification accuracy, it did not explicitly evaluate the impact of sensor placement on damage detection sensitivity or establish a

comprehensive framework that simultaneously addresses modal identification uncertainty and damage detection sensitivity. This gap highlights the need for a more integrated optimization strategy that considers both objectives within a unified framework.

Structural Health Monitoring (SHM) necessitates multi-objective optimization methods to balance competing demands, a challenge that has gained increasing attention among researchers worldwide. To address this, various studies have explored advanced optimization strategies for sensor placement. Sankary and Ostfeld [30] introduced a multi-objective approach for wireless sensor placement, enhancing the quality of modal information while minimizing energy consumption. Soman et al. [31] proposed an optimization framework that considers both structural modal identification and mode shape expansion, demonstrating its applicability to long-span bridges. Similarly, Cha et al. [32] utilized a genetic algorithm to refine the positioning of active control devices and sensors within a structural framework, achieving both cost reductions and improved control performance. Further advancements in Pareto-based sensor placement optimization have been proposed to address the complexity of multi-objective trade-offs. Nong et al. [33] developed a method incorporating Pareto optimization to simultaneously satisfy multiple modal parameter estimation criteria. This approach employed the Non-Dominated Sorting Genetic Algorithm II (NSGA-II) to efficiently compute the Pareto front, enabling the selection of sensor configurations that optimally balance competing objectives [34]. However, as the number of sensor placement evaluation criteria increases, the computational burden associated with exhaustive search methods becomes prohibitively large, rendering them impractical for large-scale structures. Consequently, intelligent algorithms have been widely adopted to identify near-optimal sensor configurations while maintaining an acceptable level of accuracy [35–37].

In this study, sensor placement criteria are separately formulated to address modal identification uncertainty and damage detection sensitivity, and a Pareto-based multi-objective optimization algorithm using the Non-Dominated Sorting Genetic Algorithm (NSGA-II) is proposed. First, Bayesian modal identification theory is applied to establish a sensor placement criterion that minimizes uncertainty in modal coordinate estimation, enhancing the accuracy and reliability of modal parameter identification. Next, leveraging the relationship between modal parameter variations and stiffness damage coefficients, a second sensor placement criterion is introduced to improve damage detection sensitivity by minimizing uncertainty in the identification of damage coefficients. To effectively balance these two competing objectives, NSGA-II is employed to construct a multi-objective optimization framework that yields a collection of Pareto-optimal sensor configurations, enabling a trade-off between modal identification accuracy and damage detectability. Finally, the proposed method is validated through numerical studies on a simply supported beam and a benchmark bridge structure, demonstrating its effectiveness in generating sensor configurations tailored to different monitoring priorities. Additionally, the interplay between modal identification uncertainty and damage detection sensitivity under identical sensor placement scenarios is analyzed to provide deeper insight into their mutual influence and trade-offs.

2. Methodology

2.1. Modal Identification Uncertainty

In general, the candidate sensor locations for a structure are selected based on the nodal positions of the corresponding finite element (FE) model. Sensors are then deployed on a subset of these candidate locations to capture response signals. However, due to measurement noise and other error factors, the structural responses recorded by sensors

may deviate from their true values. At a given sampling time t, the observed structural response, $\boldsymbol{y}(t)$, can be expressed as follows:

$$\boldsymbol{y}(t) = \boldsymbol{L}(\boldsymbol{x}(t,\boldsymbol{\theta}) + \boldsymbol{e}(t,\boldsymbol{\theta})) \tag{1}$$

where $\boldsymbol{L}$ is the sensor selection matrix, which determines the chosen sensor locations from the set of candidate positions. It is a binary matrix (composed of 0 s and 1 s), where each entry indicates whether a sensor is placed at a given location. $\boldsymbol{\theta}$ represents the parameter to be estimated; $\boldsymbol{e}(t,\boldsymbol{\theta})$ denotes the measurement noise, which accounts for the discrepancy between the observed and true structural response. Since a Gaussian distribution has the maximum entropy property, $\boldsymbol{e}(t,\boldsymbol{\theta})$ is generally considered to be a Gaussian random vector characterized by a zero mean and a covariance matrix $\boldsymbol{\Sigma}$.

We assume that structural measurements are conducted and measurement data are obtained at N discrete sampling instances, denoted as $\boldsymbol{D} = \{\boldsymbol{y}_k, k = 1, \cdots, N\}$, where k corresponds to the time step in discrete sampling. Using these sampled data along with prior information, the posterior probability density function, $p(\boldsymbol{\theta}|\boldsymbol{\Sigma},\boldsymbol{D})$, of the structural parameter is expressed as follows:

$$p(\boldsymbol{\theta}|\boldsymbol{\Sigma},\boldsymbol{D}) = c\frac{1}{\left(\sqrt{2\pi}\right)^N \sqrt{\boldsymbol{det}(\boldsymbol{\Sigma})}} \exp\left[-\frac{1}{2}\sum_{k=1}^{N}[\boldsymbol{y}_k - \boldsymbol{L}\boldsymbol{x}(\boldsymbol{\theta},k)]^T \left(\boldsymbol{L}\boldsymbol{\Sigma}\boldsymbol{L}^T\right)^{-1}[\boldsymbol{y}_k - \boldsymbol{L}\boldsymbol{x}(\boldsymbol{\theta},k)]\right] p_{\boldsymbol{\theta}}(\boldsymbol{\theta}) \tag{2}$$

where $p_{\boldsymbol{\theta}}(\boldsymbol{\theta})$ represents the prior probability distribution of the parameter; c is a normalization constant, ensuring that the right-hand side of Equation (2) integrates to 1; and $\det[\cdot]$ denotes the determinant operation. $p(\boldsymbol{\theta}|\boldsymbol{\Sigma},\boldsymbol{D})$ quantifies the uncertainty in the identified structural parameters to a certain extent. By examining the exponential term in Equation (2), it can be observed that different sensor selection matrices lead to different values of the determinant. To evaluate the effectiveness of different sensor placement configurations in improving parameter identification accuracy, an uncertainty quantification metric is required. When the total number of discrete sampling instances is sufficiently large, the asymptotic form of information entropy is employed to measure the degree of uncertainty [16]:

$$H(\boldsymbol{L}|\boldsymbol{\Sigma},\boldsymbol{D}) = \frac{1}{2}N_\theta \ln(2\pi) - \frac{1}{2}\ln[\det(\boldsymbol{Q}(\boldsymbol{L}|\boldsymbol{\theta}_0,\boldsymbol{\Sigma}))] \tag{3}$$

where $E[\cdot]$ represents the expectation operator, computing the expected value of a function, and $\ln[\cdot]$ denotes the natural logarithm operation. $H(\boldsymbol{L}|\boldsymbol{\Sigma},\boldsymbol{D})$ is the information entropy associated with a given sensor placement, quantifying the uncertainty in parameter identification. A lower entropy value indicates reduced uncertainty, enhancing the precision of identifying structural parameters. The Fisher information matrix, $\boldsymbol{Q}(\boldsymbol{L}|\boldsymbol{\theta}_0,\boldsymbol{\Sigma})$, is theoretically expanded as follows:

$$\boldsymbol{Q}(\boldsymbol{L}|\boldsymbol{\theta}_0,\boldsymbol{\Sigma}) = \sum_{k=1}^{N}\left(\boldsymbol{L}\nabla_{\boldsymbol{\theta}_0}\boldsymbol{x}(\boldsymbol{\theta},k)\right)^T\left(\boldsymbol{L}\boldsymbol{\Sigma}\boldsymbol{L}^T\right)^{-1}\left(\boldsymbol{L}\nabla_{\boldsymbol{\theta}_0}\boldsymbol{x}(\boldsymbol{\theta},k)\right) \tag{4}$$

where $\nabla_{\boldsymbol{\theta}_0}$ is the gradient matrix with respect to $\boldsymbol{\theta}_0$, which represents the optimal estimation of the structural parameter. During modal parameter identification, structural parameters are often expressed using modal coordinates ($\boldsymbol{q} = \boldsymbol{\theta}$), ensuring high precision in multi-order modal identification. The structural response is then reformulated as follows:

$$\boldsymbol{x}(\boldsymbol{\theta}) = \boldsymbol{\Phi}\boldsymbol{q} \tag{5}$$

where $\boldsymbol{\Phi}$ is the modal shape matrix of the structure, $\boldsymbol{q}$ contains modal coordinates, including natural frequencies and damping ratios for multiple modes. Reducing the estimation uncertainty of modal coordinates directly enhances the accuracy of natural frequency estimation. The best sensor placement, $\boldsymbol{L}_1$, is the one that achieves the lowest information entropy:

$$\boldsymbol{L}_1 = \underset{\boldsymbol{L}}{\operatorname{argmin}}\, H(\boldsymbol{L}\,|\boldsymbol{D}\,) = \underset{\boldsymbol{L}}{\operatorname{argmax}} \det\left((\boldsymbol{L\Phi})^T \left(\boldsymbol{L\Sigma L}^T\right)^{-1} (\boldsymbol{L\Phi}) \right) \tag{6}$$

2.2. Damage Detection Sensitivity

When using modal parameters for structural damage detection, the sensitivity of modal parameters to structural changes is crucial. The selected sensor locations should ensure that the observed modal parameters effectively reflect structural damage. In finite element simulations and dynamic equations, structural damage is typically represented by changes in stiffness. The theoretical relationship between structural damage and modal parameter variations is given as follows [8,27]:

$$(\boldsymbol{K} + \Delta\boldsymbol{K})(\boldsymbol{\Phi}_i + \Delta\boldsymbol{\Phi}_i) = (\lambda + \Delta\lambda_i)\boldsymbol{M}(\boldsymbol{\Phi}_i + \Delta\boldsymbol{\Phi}_i) \tag{7}$$

where $\boldsymbol{K}$ and $\boldsymbol{M}$ represent the stiffness matrix and mass matrix of the structure, respectively. λ_i and $\boldsymbol{\Phi}_i$ correspond to the eigenvalues and eigenvectors of the i-th mode. The operator Δ denotes variations in these parameters due to structural damage. By expanding Equation (7) and normalizing the mode shape using the mass matrix, while neglecting higher-order small terms, the changes in natural frequencies and mode shapes can be expressed as follows:

$$f_i = \frac{\boldsymbol{\Phi}_i^T \Delta\boldsymbol{K} \boldsymbol{\Phi}_i}{8 \cdot f_i \cdot \pi^2} \tag{8}$$

$$\Delta\boldsymbol{\Phi}_i = \sum_{r=1}^{m} -\frac{\boldsymbol{\Phi}_r^T \Delta\boldsymbol{K} \boldsymbol{\Phi}_i}{4\pi^2 \left(f_r^2 - f_i^2\right)} \boldsymbol{\Phi}_r \tag{9}$$

where f_i and f_r represent the i-th and r-th natural frequencies, and m denotes the modal order under consideration. Variations in the stiffness matrix coefficients of individual elements serve as indicators of structural damage:

$$\Delta\boldsymbol{K} = \sum_{j=1}^{N_e} \beta_j \boldsymbol{K}_j \tag{10}$$

where N_e is the number of stiffness matrix elements, and $\boldsymbol{K}_j$ represents the contribution of the j-th element to the overall stiffness matrix. β_j is the damage coefficient, a scalar between 0 and 1, indicating the degree of damage in the j-th element. The variations in modal parameters can be further rewritten as

$$\Delta f_i = \left[\frac{\boldsymbol{\Phi}_i^T \boldsymbol{K}_1 \boldsymbol{\Phi}_i}{8 \cdot f_i \cdot \pi^2}, \cdots, \frac{\boldsymbol{\Phi}_i^T \boldsymbol{K}_{N_e} \boldsymbol{\Phi}_i}{8 \cdot f_i \cdot \pi^2} \right] [\beta_1, \cdots, \beta_{N_e}]^T = \boldsymbol{F_i \beta} \tag{11}$$

$$\Delta\boldsymbol{\Phi}_i = \left[\sum_{\substack{r=1 \\ r \neq i}}^{N_d} \frac{-\boldsymbol{\Phi}_r^T \boldsymbol{K}_1 \boldsymbol{\Phi}_i}{\lambda_r - \lambda_i} \boldsymbol{\Phi}_r, \cdots, \sum_{\substack{r=1 \\ r \neq i}}^{N_d} \frac{-\boldsymbol{\Phi}_r^T \boldsymbol{K}_{N_e} \boldsymbol{\Phi}_i}{\lambda_r - \lambda_i} \boldsymbol{\Phi}_r \right] [\beta_1, \cdots, \beta_{N_e}]^T = \boldsymbol{E}_i \boldsymbol{\beta} \tag{12}$$

where $\boldsymbol{\beta}$ is the structural damage coefficient vector, and $\boldsymbol{F}_i$ and $\boldsymbol{E}_i$ are the sensitivity coefficient vectors of natural frequencies and mode shapes with respect to $\boldsymbol{\beta}$. Equations (11) and (12)

describe the sensitivity of modal parameters to structural damage. Notably, Equation (11) is independent of the sensor selection matrix, implying that reducing the uncertainty estimation is directly linked to frequency estimation accuracy, which is addressed in Section 2.1. Conversely, Equation (12) reveals that the observed mode shape variations depend significantly on sensor placement. Its mathematical form is similar to Equation (6), allowing it to be reformulated as

$$\Delta\hat{\boldsymbol{\Phi}} = \boldsymbol{L}(\Delta\boldsymbol{\Phi}(\boldsymbol{\beta}) + \boldsymbol{e}(\boldsymbol{\beta})) \tag{13}$$

where $\Delta\hat{\boldsymbol{\Phi}}$ is the observed mode shape variation, and $\Delta\boldsymbol{\Phi}(\boldsymbol{\beta})$ represents the actual mode shape variation. $\boldsymbol{e}(\boldsymbol{\beta})$ denotes the observation noise, with the i-th column corresponding to the i-th mode's measurement error. Assuming a Gaussian noise model with zero mean and variance $\boldsymbol{\Sigma}_i$, the optimal sensor placement should minimize the entropy of damage coefficient estimation uncertainty. Thus, the best sensor placement $\boldsymbol{L}_2$ is the one that achieves the lowest information entropy:

$$\boldsymbol{L}_2 = \underset{\boldsymbol{L}}{\operatorname{argmin}}\, H\left(\boldsymbol{L}\middle|\Delta\hat{\boldsymbol{\Phi}}\right) = \underset{\boldsymbol{L}}{\operatorname{argmax}} \sum_{i=1}^{m} \det\left((\boldsymbol{L}\boldsymbol{E}_i)^T\left(\boldsymbol{L}\boldsymbol{\Sigma}_i\boldsymbol{L}^T\right)^{-1}(\boldsymbol{L}\boldsymbol{E}_i)\right) \tag{14}$$

2.3. Multi-Objective Optimization Method

In sensor placement optimization, when both modal identification uncertainty and damage detection sensitivity must be considered simultaneously, single-objective optimization methods often fail to effectively balance these competing factors. To address this challenge, Pareto optimization is introduced to establish a multi-objective sensor placement criterion, allowing for a comprehensive evaluation of how these two objectives influence the optimal sensor configuration. The core concept of Pareto optimization is to solve for the Pareto front, which yields a collection of non-dominated solutions, capturing the trade-offs between the two objectives rather than converging to a single globally optimal outcome. The Pareto front ensures that no other solution can simultaneously outperform a given solution in both objectives, thereby providing multiple optimized sensor placement strategies for decision-making. However, solving for the Pareto front poses significant computational challenges. Traditional global search algorithms often involve excessive computational costs, while sequential optimization methods tend to become trapped in local optima. To improve computational efficiency and obtain high-quality sensor placement solutions, this study employs the NSGA-II. The proposed approach consists of four key steps:

(1) Discrete Encoding of Candidate Sensor Locations: A set of finite element model nodes are selected as candidate measurement positions, ensuring that potential sensor locations are well distributed across the structure. To represent sensor placement decisions, a binary encoding scheme (0, 1) is adopted, where '1' indicates that a sensor is placed at a given node and '0' means no sensor is placed at that node. This encoding forms the sensor selection matrix $\boldsymbol{L}$, which is shown in Equation (1).

(2) Initial Population Generation and Evolution: An initial population of sensor placement configurations is randomly generated, and their bi-objective function values are computed. Through selection, crossover, and mutation operations, new solutions are iteratively generated, allowing the population to evolve over successive generations.

(3) Non-Dominated Sorting and Crowding Distance Computation: the parent and offspring populations are merged, and non-dominated sorting, along with crowding distance measures, is applied to select superior individuals, maintaining both the quality and diversity of Pareto front solutions.

(4) Convergence Assessment and Termination: The process is repeated until a termination threshold is reached, either upon hitting the maximum generation count or when

population convergence is achieved. If the termination criterion is not satisfied, the optimization process continues until a stable Pareto front solution set is obtained.

By leveraging this multi-objective optimization framework, a reasonable balance between modal identification uncertainty and damage detection sensitivity can be achieved. The proposed approach provides an optimized sensor placement strategy for SHM applications, facilitating more efficient and reliable monitoring of engineering structures.

3. Case Study Analysis

3.1. The Simply Supported Beam

The proposed sensor placement method is first applied to a simply supported beam numerical model to analyze the characteristics of sensor distributions corresponding to modal identification uncertainty and damage detection sensitivity. Additionally, the mutual influence between these two objectives on sensor placement is investigated. The simply supported beam model has a Young's modulus of 212 GPa, a density of 7456 kg/m^3, and cross-sectional dimensions of 50 mm $\times$ 15.62 mm [29]. The beam has a total length of 1.9 m and is discretized into 19 finite elements using planar beam elements ($N_e = 19$). As shown in Figure 1, the 18 vertical degrees of freedom (DOFs) at the nodes serve as candidate sensor locations. The first three modal shapes are selected as the target modes for identification. Since Rayleigh damping preserves the mode shapes for both damped and undamped cases, the damping effect does not influence the mode shape selection. To ensure accurate modal identification, the number of sensors must exceed the number of target modes. Thus, the number of deployed sensors is set to five to ensure adequate monitoring coverage, with the objective functions defined as follows: Objective Function 1 focuses on minimizing modal identification uncertainty, as formulated in Equation (6), while Objective Function 2 aims to maximize damage detection sensitivity, as formulated in Equation (14).

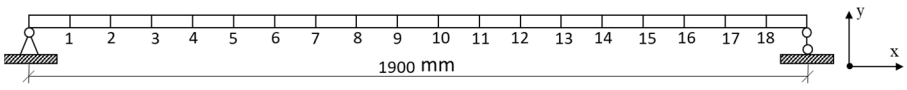


Figure 1. Numbering of candidate sensor locations on a simply supported beam.

Figure 2 presents the distribution of nine Pareto-optimal solutions, where the horizontal axis represents Objective Function 1 (modal identification uncertainty) and the vertical axis represents Objective Function 2 (damage detection sensitivity). In the figure, red-filled circles denote Pareto front solutions, while blue-filled circles indicate locally optimal solutions obtained during the optimization process. By analyzing the Pareto front and locally optimal solutions, along with the better and worse trade-off directions, it is evident that no solution on the Pareto front is simultaneously outperformed in both objectives. The specific number of nine solutions is not pre-determined but rather emerges from the convergence process of the optimization algorithm. In general, the greater the number of candidate sensor locations and the larger the variations in different modal shapes, the more complex the model becomes in the algorithm's computation. This increases the likelihood of falling into local optima, making it necessary to run the algorithm multiple times to capture as many Pareto front solutions as possible. Additionally, when no clear preference exists between the two objectives, solutions on the Pareto front cannot be directly ranked as superior or inferior. The Pareto front exhibits a downward trend from the upper left to the lower right, indicating an inherent trade-off relationship; optimizing one objective typically leads to the deterioration of the other. To illustrate different trade-off scenarios, three representative solutions (Case A, Case B, and Case C) are marked in Figure 2. Case A prioritizes modal identification uncertainty reduction, but at the expense of lower damage detection sensitivity. Case C prioritizes damage

detection sensitivity, resulting in increased modal identification uncertainty. Case B represents a compromise solution, balancing both objectives.

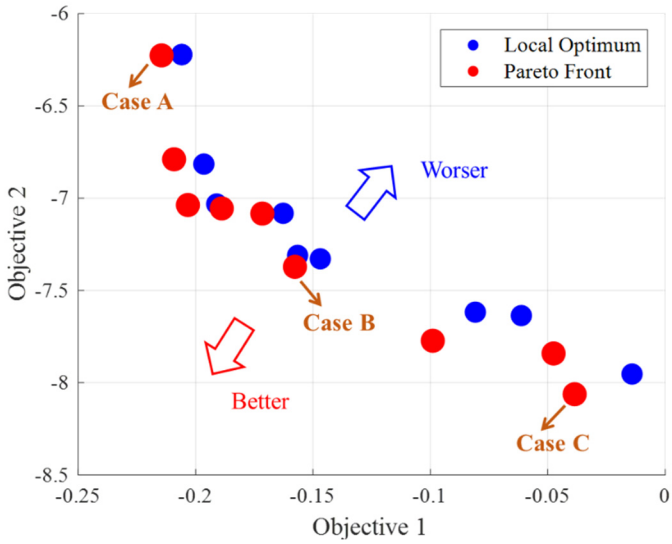


Figure 2. Pareto front based on bi-objective function.

Figure 3 visualizes the sensor placement configurations corresponding to Case A, Case B, and Case C, where brown arrows indicate the selected sensor locations. The sensor distributions reflect different trade-off orientations within the multi-objective optimization framework. Case A (minimizing modal identification uncertainty): Sensors are concentrated at positions 5, 10–12, and 18, particularly covering critical modal response regions, such as the mid-span and support areas. This layout enhances the stability of modal parameter identification, making it suitable for applications emphasizing global vibration characteristics and modal parameter estimation. Case C (maximizing damage detection sensitivity): Sensors are positioned towards the central region of the beam, specifically at positions 6–13, to capture local damage characteristics more effectively. This configuration improves the ability to detect stiffness changes and small-scale structural damage, making it ideal for damage-sensitive monitoring applications. Case B (balanced trade-off solution): Sensors are more evenly distributed, covering positions 1, 3, 5, 6, 10, 12, 16, and 18, ensuring both stable modal identification and enhanced damage detection capability. This configuration achieves a balance between global and local monitoring objectives, making it suitable for scenarios requiring both structural integrity assessment and damage sensitivity.

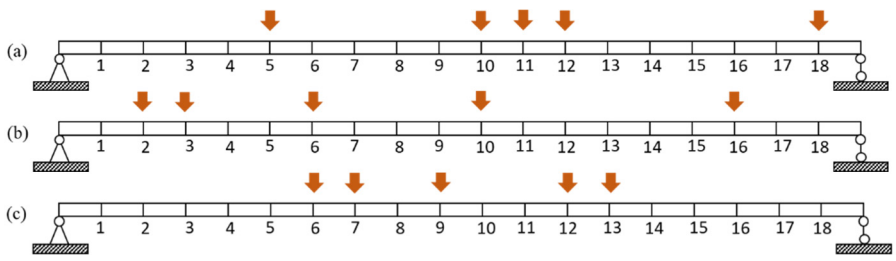


Figure 3. Sensor placement corresponding to different pareto fronts: (**a**) Case A; (**b**) Case B; (**c**) Case C.

Figure 4 provides a statistical analysis of sensor selection frequency across Pareto-optimal solutions: Figure 4a corresponds to the top four Pareto-optimal solutions for modal identification uncertainty; Figure 4b corresponds to the top four solutions for damage detection sensitivity. The horizontal axis represents sensor locations, while the vertical axis indicates the frequency of selection for each location across multiple Pareto-

optimal solutions. Numbers in parentheses (e.g., (69, 3)) denote the number of times a specific location was chosen. From Figure 4a, it is evident that modal identification-focused optimization results in a more distributed sensor placement, with frequently selected locations being 8, 11, 12, 15, 16, and 18. Conversely, Figure 4b shows that damage detection-focused optimization concentrates sensors in specific locations, particularly 3, 6, 9, 10, 14, and 16, where localized damage sensitivity is higher. This further confirms that the two objectives mutually influence the sensor placement strategy—certain locations are favored in one optimization scheme but may be less significant in the other.

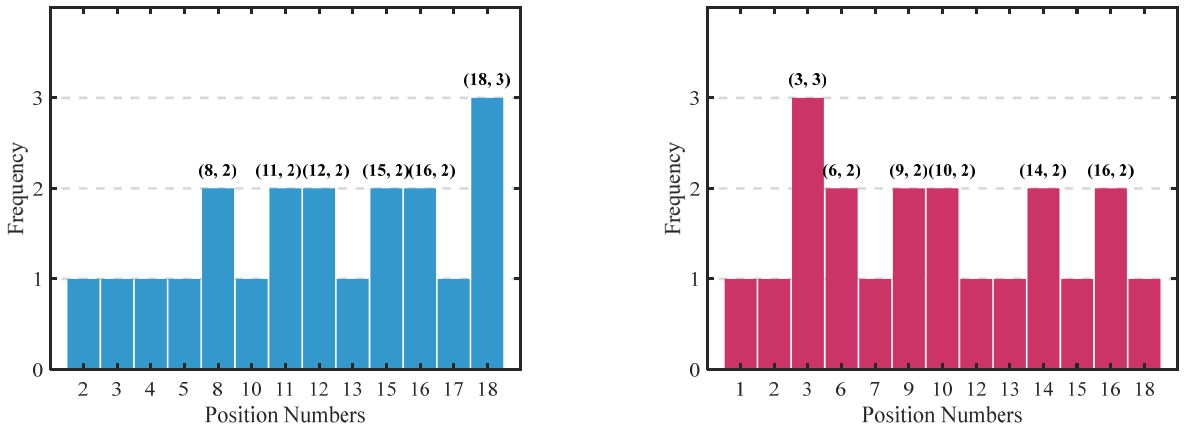


Figure 4. Pareto front sensor placement for single-objective function preference: (**a**) Objective 1; (**b**) Objective 2.

3.2. The Bridge Benchmark Structure

To further validate the effectiveness of the proposed method, a benchmark bridge model developed by the University of Central Florida is employed. This model has been widely utilized in research related to modal identification and damage detection [29,38]. Figure 5a presents a physical view of the benchmark bridge model, which is constructed using spatial beam elements and consists of 182 structural elements. The vertical direction (Z-axis) is considered the primary direction of interest, and the first three Z-directional modal shapes are selected for identification. The nodes on the bridge deck serve as candidate sensor locations, and Figure 5b illustrates their numbering sequence. Compared to the previous simply supported beam model, where only five sensors were deployed, ten sensors are allocated in this case to better observe their spatial distribution within a more complex structural system. The two objective functions used for optimization are formulated based on Equations (6) and (14), respectively.

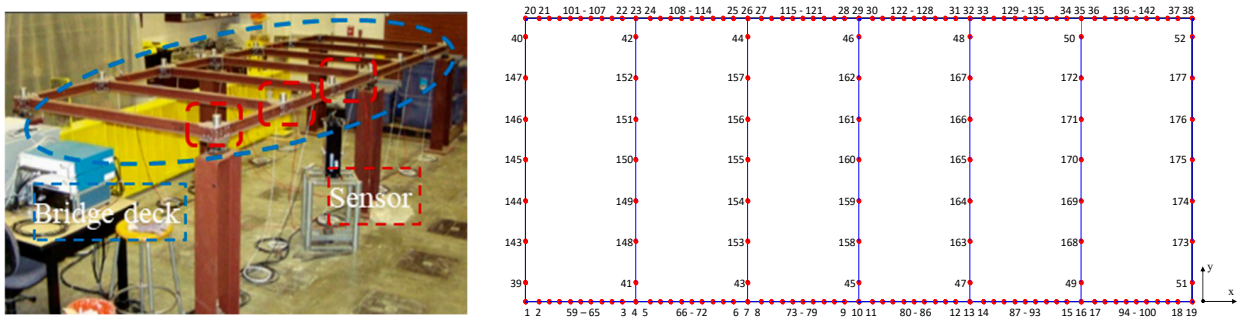


Figure 5. The bridge benchmark structure: (**a**) physical model diagram; (**b**) numbering of candidate measurement points.

Figure 6 depicts the distribution of seven Pareto-optimal solutions, where the horizontal axis represents Objective Function 1 (modal identification uncertainty) and the vertical axis represents Objective Function 2 (damage detection sensitivity). Red-filled circles indicate Pareto front solutions, whereas blue-filled circles represent locally optimal solutions obtained during the optimization process. Analyzing the Pareto front and locally optimal solutions, along with the direction of the better and worse trade-offs, reveals that no solution on the Pareto front can be simultaneously outperformed in both objectives. Compared to Figure 2, the proportion of locally optimal solutions is significantly higher in Figure 6, primarily due to the higher complexity of the benchmark bridge model compared to the simpler simply supported beam model. This increased complexity limits the capability of the optimization algorithm to reach global optima, often resulting in suboptimal solutions. Additionally, when no clear preference exists between the two objectives, the solutions on the Pareto front cannot be directly ranked as superior or inferior. The Pareto front exhibits a downward trend from the upper left to the lower right, indicating an inherent trade-off relationship; improving one objective typically leads to the deterioration of the other. Similarly to Figure 2, three representative cases (Case A, Case B, and Case C) are marked in the figure. Case A corresponds to a solution where modal identification uncertainty is minimized, but at the cost of reduced damage detection sensitivity. Conversely, Case C prioritizes damage detection sensitivity, resulting in a higher modal identification uncertainty. Case B, situated between the two extremes, provides a balanced trade-off and serves as a compromise solution between both objectives.

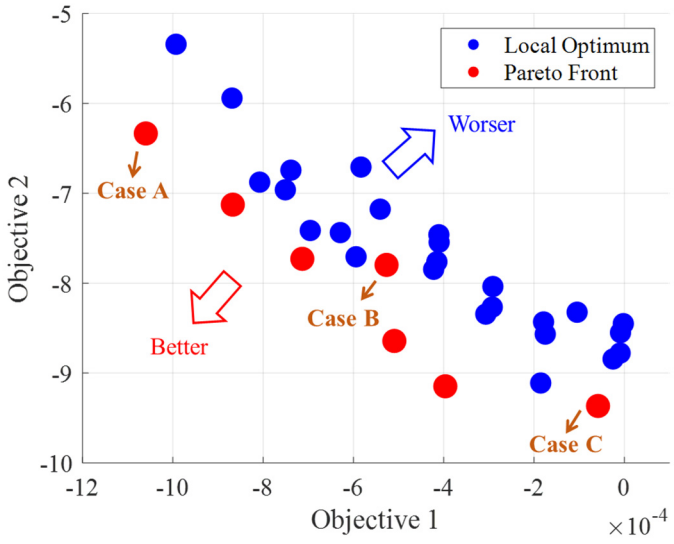


Figure 6. Pareto front based on bi-objective function.

Figure 7 illustrates the sensor placement configurations corresponding to different optimization preferences, where brown arrows indicate the selected sensor locations. The distribution patterns reflect distinct optimization priorities within the multi-objective framework. In Case A, sensors are predominantly placed along the edges, support regions, and certain mid-span locations (e.g., sensors at positions 44, 160, and 45). This configuration is well suited for capturing the global vibrational response, thereby reducing modal identification uncertainty and improving the accuracy of modal parameter estimation. Such a distribution is ideal for applications emphasizing global structural behavior characterization. In Case C, sensor placement is more concentrated in the web region and other critical localized areas (e.g., positions 41, 43, 45, and 159), with additional sensors near beam ends and support locations. This setup enhances damage detection sensitivity, making it more effective in identifying small-scale damage or local stiffness variations and making it particularly suitable

for damage-sensitive monitoring scenarios. Case B serves as a compromise configuration, balancing global modal identification accuracy and local damage sensitivity. Sensors are distributed across the edges, mid-span, and support areas, ensuring stable modal identification while also improving damage detection capabilities. This configuration is particularly useful in applications where a balanced monitoring strategy is required.

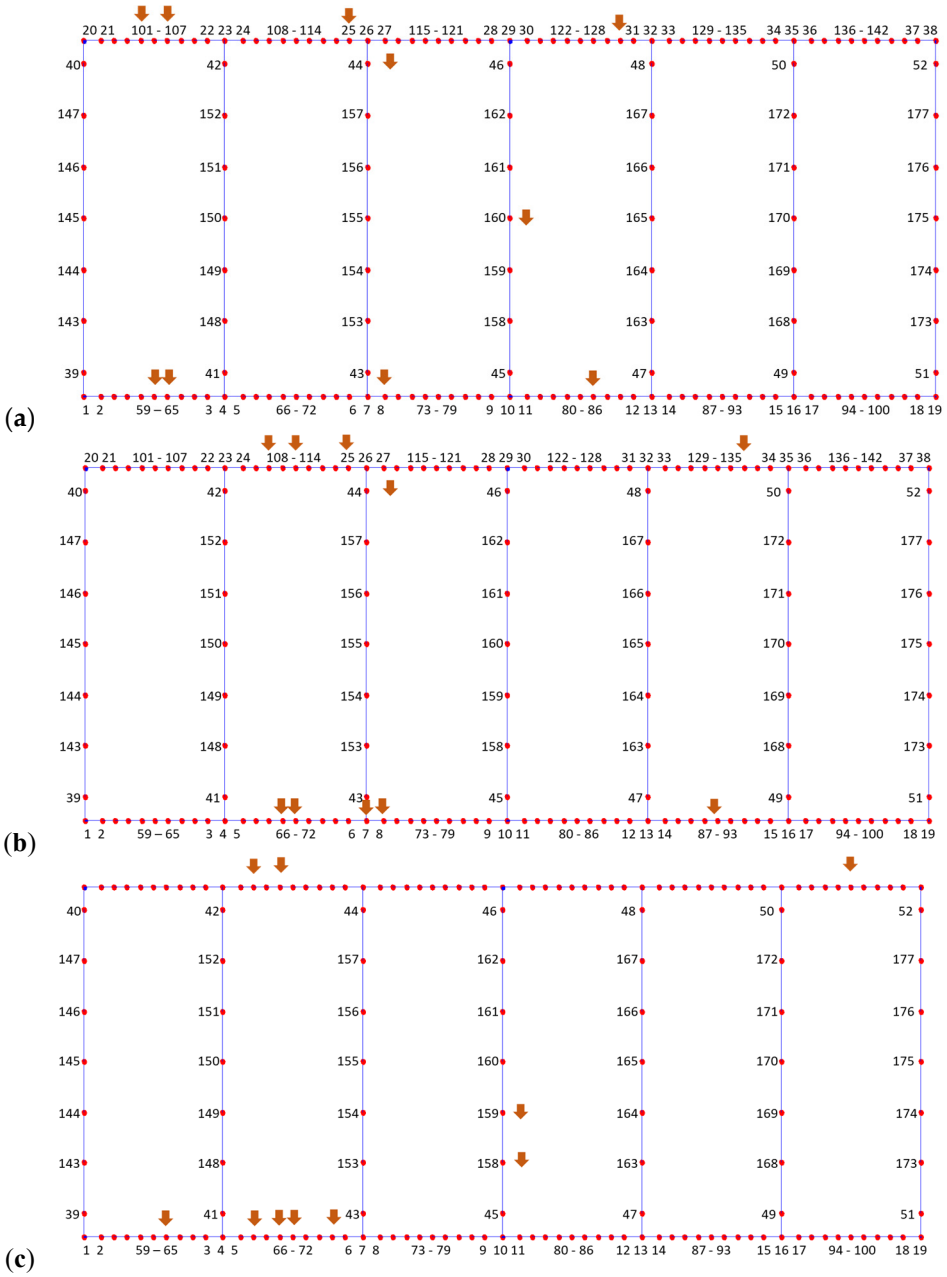
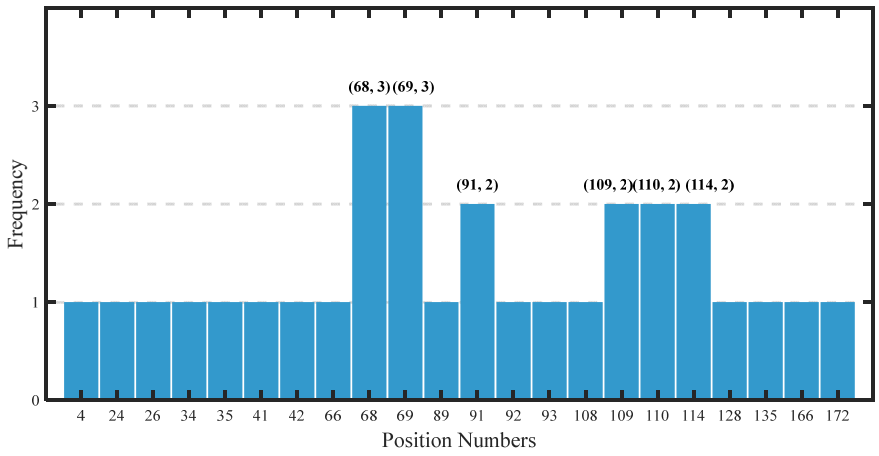


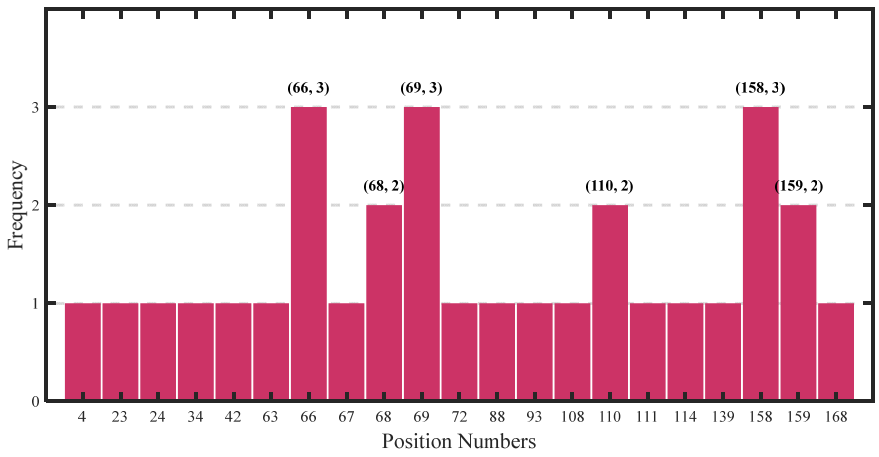
Figure 7. Sensor placement corresponding to different pareto fronts: (**a**) Case A; (**b**) Case B; (**c**) Case C.

Figure 8 presents a statistical analysis of sensor selection frequency across different Pareto-optimal solutions. Figure 8a corresponds to the top three Pareto-optimal solutions for modal identification uncertainty, while Figure 8b corresponds to the top three solutions for damage detection sensitivity. The horizontal axis represents sensor locations, and the vertical axis indicates the number of times a given location was selected across multiple Pareto-optimal solutions. The numbers in parentheses denote the frequency of selection for each location. From Figure 8a, it is evident that modal identification-focused optimization results in a more dispersed sensor distribution, primarily covering locations 68, 69, 91,

109, 110, and 114. Among these, locations 68 and 69 were selected three times, indicating their significant contribution to reducing modal identification uncertainty and ensuring the stability of global modal responses. In contrast, Figure 8b demonstrates that damage detection-focused optimization produces a more localized sensor distribution, with sensors concentrated at locations 66, 68, 69, 110, 158, and 159. Notably, locations 66, 69, and 158 were selected three times, highlighting their high sensitivity to localized damage and their ability to capture small-scale structural anomalies. Compared to modal identification optimization, damage detection optimization results in sensor placement that is more focused on key regions, particularly around locations 66, 69, and 158. From an overall perspective, modal identification-driven sensor layouts tend to cover a broader range of locations, ensuring a more evenly distributed placement that enhances global response estimation. In contrast, damage detection-driven layouts prioritize localized key areas, improving the sensitivity to structural anomalies. Additionally, some locations—such as positions 68, 69, and 110—were frequently selected in both optimization strategies, suggesting that they play a critical role in achieving both objectives. In practical engineering applications, the sensor placement strategy can be adjusted based on the specific monitoring priorities, ensuring an optimal balance between global modal estimation accuracy and localized damage detection sensitivity.



(**a**)



(**b**)

Figure 8. Pareto front sensor placement for single-objective function preference: (**a**) Objective 1; (**b**) Objective 2.

3.3. Discussion

In the finite element model of a structure, changes in the stiffness matrix are typically used to represent structural variations. Generally, the overall stiffness matrix change is obtained by accumulating the changes in individual element stiffness matrices, which are typically caused by material degradation or constraint variations, both of which are reflected in the variation coefficients of the element stiffness matrices. In our study, we simulate structural damage by reducing the stiffness of selected finite element components in both the simply supported beam model and the benchmark bridge model according to damage coefficients. In damage detection research, it is commonly assumed that the damage coefficient lies between 0.1 and 0.3. Notably, when the covariance matrix is assumed to be a diagonal matrix with equal diagonal elements, the absolute values of the assumed damage coefficients do not affect the relative ranking of different sensor placements. Furthermore, Equation (14) is a simplified form, assuming that the variations in different stiffness matrix coefficients are similar. If there are significant differences in the variation patterns, Equation (13) can be used to derive the partial derivative of the damage coefficient, which can then be substituted into Equation (4) for further analysis.

Previous studies on structural parameter identification (including modal and physical parameters) have examined the impact of damage on parameter estimation and further evaluated its influence on sensor placement strategies. The findings indicate that when damage detection sensitivity is not considered and only parameter identification uncertainty is considered in a single-objective framework, the presence of structural damage has little impact on sensor placement [29]. On the one hand, in computational analysis, the effect of damage is often modeled as variations in noise variance or as a random distribution. These assumptions do not introduce significant fluctuations into the data distribution and, consequently, do not lead to substantial differences in the computational results [13,17,24,27,28]. On the other hand, as observed in this study, even when damage effects are considered, the optimization criteria remain focused on structural parameter estimation, fundamentally maintaining a single-objective optimization framework. Since the objective function remains unchanged and the structural information contained in the selected sensor locations varies only slightly, the sensor placement strategy remains largely unaffected. However, the multi-objective optimization approach proposed in this study reveals that the selection of sensor locations is influenced by the interplay between the two objectives. Given that different objective functions exhibit distinct computational tendencies, the information captured at different sensor locations also varies, leading to an interdependent selection process. It is important to note that this interaction does not always manifest as a conflicting relationship, as it depends on the definition of the objective functions and the correlation between the data used in the computation.

4. Conclusions

This study proposes a multi-objective sensor placement method based on the NSGA-II to balance modal identification uncertainty and damage detection sensitivity in SHM. By introducing information entropy to quantify the uncertainty in both modal coordinate estimation and stiffness variation assessment, the method provides a systematic framework for optimizing sensor layouts. Numerical validation on a simply supported beam and a benchmark bridge structure confirms its effectiveness in generating sensor configurations tailored to different monitoring priorities.

A key innovation of this study is the use of information entropy to evaluate the uncertainty in stiffness variation estimation, which enhances the assessment of damage detection sensitivity. By integrating this approach within the optimization framework, the method enables a more robust and adaptive selection of sensor placements, improving both

the accuracy and reliability of structural damage identification. The results show that sensor layouts optimized for damage detection tend to cluster in regions where stiffness changes are most pronounced, effectively enhancing sensitivity to localized structural deterioration. Conversely, configurations prioritizing modal identification are more evenly distributed, ensuring comprehensive modal response capture but potentially reducing sensitivity to local damage. This interplay highlights the inherent trade-off between the two objectives, where optimizing one may come at the expense of the other.

Additionally, the Pareto-based optimization framework provides a range of trade-off solutions, allowing engineers to select sensor placements that best align with specific monitoring requirements. The results indicate that while balanced sensor distributions ensure adequate performance for both objectives, targeted configurations can be fine-tuned to either enhance modal identification accuracy or increase sensitivity to structural damage. This adaptability ensures that the method can be effectively applied to various SHM scenarios with different constraints and priorities.

Due to time and capability constraints, there are still areas in this study that can be further explored. Future research could incorporate physical parameter identification, time-series prediction, and correlation analysis to formulate additional objective functions. By utilizing Pareto optimization methods, the interactions between different monitoring objectives in sensor placement can be analyzed, leading to further optimization of sensor placement strategies.

Author Contributions: Conceptualization, X.-Y.P.; methodology, X.-Y.P. and J.-X.Z.; software, Y.H. and H.-B.H.; validation, J.-X.Z. and H.-B.H.; formal analysis, J.-X.Z.; investigation, X.-Y.P.; data curation, X.-Y.P. and H.-B.H.; writing—original draft preparation, X.-Y.P. and Y.H.; writing—review and editing X.-Y.P. and J.-X.Z.; funding acquisition, X.-Y.P. and H.-B.H. All authors have read and agreed to the published version of the manuscript.

Funding: This research work was jointly supported by the National Natural Science Foundation of China (Grant No. 52108287) and the Tiankai Higher Education Science and Technology Innovation Park Enterprise R&D Special Project (Grant No. 23YFZXYC00026).

Data Availability Statement: Some or all of the data models that support the findings of this study are available from the corresponding author upon reasonable request.

Conflicts of Interest: The authors declare no conflicts of interest.

References

1. Farrar, C.R.; Worden, K. An introduction to structural health monitoring. *Philos. Trans. R. Soc. A Math. Phys. Eng. Sci.* **2006**, *365*, 303–315. [CrossRef] [PubMed]
2. Mishra, M.; Lourenço, P.B.; Ramana, G.V. Structural health monitoring of civil engineering structures by using the internet of things: A review. *J. Build. Eng.* **2022**, *48*, 103954. [CrossRef]
3. Reynders, E. System identification methods for (operational) modal analysis: Review and comparison. *Arch. Comput. Methods Eng.* **2012**, *19*, 51–124. [CrossRef]
4. Huang, H.B.; Yi, T.H.; Li, H.N. Bayesian combination of weighted principal component analysis for diagnosing sensor faults in structural monitoring systems. *J. Eng. Mech.* **2017**, *143*, 04017088. [CrossRef]
5. Frigui, F.; Faye, J.P.; Martin, C.; Dalverny, O.; Peres, F.; Judenherc, S. Global methodology for damage detection and localization in civil engineering structures. *Eng. Struct.* **2018**, *171*, 686–695. [CrossRef]
6. Avci, O.; Abdeljaber, O.; Kiranyaz, S.; Hussein, M.; Gabbouj, M.; Inman, D.J. A review of vibration-based damage detection in civil structures: From traditional methods to machine learning and deep learning applications. *Mech. Syst. Signal Process.* **2021**, *147*, 107077. [CrossRef]
7. Yi, T.H.; Li, H.N.; Gu, M. Sensor placement for structural health monitoring of Canton Tower. *Smart Struct. Syst.* **2012**, *10*, 313–329. [CrossRef]
8. Yin, T.; Zhu, H.; Yu, L. Noise analysis for sensitivity-based structural damage detection. *Appl. Math. Mech.* **2007**, *28*, 741–750. [CrossRef]
9. Cao, X.; Chen, J.; Xu, Q.; Li, J. A distance coefficient-multi objective information fusion algorithm for optimal sensor placement in structural health monitoring. *Adv. Struct. Eng.* **2021**, *24*, 718–732. [CrossRef]

10. Nicoletti, V.; Quarchioni, S.; Amico, L.; Gara, F. Assessment of different optimal sensor placement methods for dynamic monitoring of civil structures and infrastructures. *Struct. Infrastruct. Eng.* **2024**, 1–16. [CrossRef]
11. Taher, S.A.; Li, J.; Fang, H. Simultaneous seismic input and state estimation with optimal sensor placement for building structures using incomplete acceleration measurements. *Mech. Syst. Signal Process.* **2023**, *188*, 110047. [CrossRef]
12. Garbowski, T.; Cornaggia, A.; Zaborowicz, M.; Sowa, S. Computer-Aided Structural Diagnosis of Bridges Using Combinations of Static and Dynamic Tests: A Preliminary Investigation. *Materials* **2023**, *16*, 7512. [CrossRef] [PubMed]
13. Kammer, D.C. Effect of model error on sensor placement for on-orbit modal identification of large space structures. *J. Guid. Control. Dyn.* **1992**, *15*, 334–341. [CrossRef]
14. Kammer, D.C.; Tinker, M.L. Optimal placement of triaxial accelerometers for modal vibration tests. *Mech. Syst. Signal Process.* **2004**, *18*, 29–41. [CrossRef]
15. Li, D.S.; Li, H.N.; Fritzen, C.P. The connection between effective independence and modal kinetic energy methods for sensor placement. *J. Sound Vib.* **2007**, *305*, 945–955. [CrossRef]
16. Papadimitriou, C.; Beck, J.L.; Au, S.K. Entropy-based optimal sensor location for structural model updating. *J. Vib. Control.* **2000**, *6*, 781–800. [CrossRef]
17. Papadimitriou, C.; Lombaert, G. The effect of prediction error correlation on optimal sensor placement in structural dynamics. *Mech. Syst. Signal Process.* **2012**, *28*, 105–127. [CrossRef]
18. Pei, X.Y.; Yi, T.H.; Li, H.N. A multitype sensor placement method for the modal estimation of structure. *Smart Struct. Syst.* **2018**, *21*, 407–420. [CrossRef]
19. Zhang, C.D.; Xu, Y.L. Optimal multi-type sensor placement for response excitation reconstruction. *J. Sound Vib.* **2016**, *360*, 112–128. [CrossRef]
20. Huang, J.Z.; Li, D.S.; Li, H.N. A new regime-switching cointegration method for structural health monitoring under changing environmental and operational conditions. *Measurement* **2023**, *212*, 112682. [CrossRef]
21. Pei, X.Y.; Huang, H.B.; Cao, P. An Improved Gaussian Mixture Model-Based Data Normalization Method for Removing Environmental Effects on Damage Detection of Structures. *Buildings* **2025**, *15*, 359. [CrossRef]
22. Roy, K.; Samit, R.C. Fundamental mode shape and its derivatives in structural damage localization. *J. Sound Vib.* **2013**, *332*, 5584–5593. [CrossRef]
23. Yoon, M.K.; Heider, D.; Gillespie, J.W.; Ratcliffe, C.P.; Crane, R.M. Local damage detection with the global fitting method using mode shape data in notched beams. *J. Nondestruct. Eval.* **2009**, *28*, 63–74. [CrossRef]
24. Yang, W.; Sun, L.M.; Yu, G. Optimal sensor placement methodology for uncertainty reduction in the assessment of structural condition. *Struct. Control. Health Monit.* **2016**, *24*, e1927. [CrossRef]
25. Hiramoto, K.; Doki, H.; Obinata, G. Optimal sensor/actuator placement for active vibration control using explicit solution of algebraic Riccati equation. *J. Sound Vib.* **2000**, *229*, 1057–1075. [CrossRef]
26. Worden, K.; Burrows, A.P. Optimal sensor placement for fault detection. *Eng. Struct.* **2001**, *23*, 885–901. [CrossRef]
27. Shi, Z.Y.; Law, S.S.; Zhang, L.M. Optimum sensor placement for structuraldamage detection. *J. Eng. Mech.* **2000**, *126*, 1173–1179. [CrossRef]
28. Guo, H.Y.; Zhang, L.; Zhang, L.L.; Zhou, J. Optimal placement of sensors for structural health monitoring using improved genetic algorithms. *Smart Mater. Struct.* **2004**, *13*, 528. [CrossRef]
29. Pei, X.Y.; Yi, T.H.; Qu, C.X.; Li, H.-N. Conditional information entropy based sensor placement method considering separated model error and measurement noise. *J. Sound Vib.* **2019**, *449*, 389–404. [CrossRef]
30. Sankary, N.; Ostfeld, A. Multiobjective Optimization of Inline Mobile and Fixed Wireless Sensor Networks under Conditions of Demand Uncertainty. *J. Water Resour. Plan. Manag.* **2018**, *144*, 04018043. [CrossRef]
31. Soman, R.N.; Onoufriou, T.; Kyriakides, M.A.; Votsis, R.A.; Chrysostomou, C.Z. Multi-type, multi-sensor placement opti-mization for structural health monitoring of long span bridges. *Smart Struct. Syst.* **2014**, *14*, 55–70. [CrossRef]
32. Cha, Y.; Raich, A.; Barroso, L.; Agrawal, A. Optimal placement of active control devices and sensors in frame structures using multi-objective genetic algorithms. *Struct. Control. Heal. Monit.* **2011**, *20*, 16–44. [CrossRef]
33. Nong, S.X.; Yang, D.H.; Yi, T.H. Pareto-based bi-objective optimization method of sensor placement in structural health monitoring. *Buildings* **2021**, *11*, 549. [CrossRef]
34. Srinivas, N.; Deb, K. Multiobjective optimization using non-dominated sorting in genetic algorithms. *Evol. Comput.* **1994**, *2*, 221–248. [CrossRef]
35. Ahlawat, A.S.; Ramaswamy, A. Multiobjective Optimal Structural Vibration Control Using Fuzzy Logic Control System. *J. Struct. Eng.* **2001**, *127*, 1330–1337. [CrossRef]
36. Rao, A.R.M.; Anandakumar, G. Optimal placement of sensors for structural system identification and health monitoring using a hybrid swarm intelligence technique. *Smart Mater. Struct.* **2007**, *16*, 2658–2672. [CrossRef]
37. Yi, T.-H.; Li, H.-N.; Song, G.; Zhang, X.-D. Optimal sensor placement for health monitoring of high-rise structure using adaptive monkey algorithm. *Struct. Control Health Monit.* **2015**, *22*, 667–681. [CrossRef]
38. Caicedo, J.M.; Catbas, N.; Gul, M.; Zaurin, R.; Dyke, S.J. Benchmark problem for bridge health monitoring: Definition paper. In Proceedings of the 4th World Conference on Structural Control and Monitoring, San Diego, CA, USA, 11–13 July 2006.

Disclaimer/Publisher's Note: The statements, opinions and data contained in all publications are solely those of the individual author(s) and contributor(s) and not of MDPI and/or the editor(s). MDPI and/or the editor(s) disclaim responsibility for any injury to people or property resulting from any ideas, methods, instructions or products referred to in the content.